nature communications

Article

https://doi.org/10.1038/s41467-024-55180-3

Phase-transition-induced dynamic surface wrinkle pattern on gradient photo-crosslinking liquid crystal elastomer

Received: 20 May 2024

Accepted: 4 December 2024

Published online: 30 December 2024

Check for updates

Tao Wen[1,2], Tianjiao Ma[2] ✉, Jie Qian[2], Zhaoxin Song[3], Xuesong Jiang[2] ✉ & Yuan Yao[1] ✉

Liquid crystal elastomers (LCEs) with various deformation properties based on phase transition were widely used as actuators and provided potential to fabricate functional surfaces with tunable microstructure. Herein, we demonstrate a strategy to fabricate dynamic micro wrinkles on LCE surfaces based on LC phase transition. Stable micron-sized surface wrinkles on the anthracene-containing LCE film (AnLCE) are fabricated by ultraviolet exposure induced gradient cross-linking and subsequently stretching-releasing (UV-SR). The surface wrinkle is stabilized by the orientation of liquid crystal mesogens in the crosslinked top layer, while it can be erased by heating due to the isotropic phase-transition and recovered by stretching-releasing again. The dynamic natures cooperated with multi display modes under natural light, UV light and polarized light enable wrinkled AnLCE as a dynamic and multi-mode display platform. This strategy provide a path for modifying LCEs and regulating surface polarized images via wrinkling, which may be potential in soft sensors and optics, smart windows and anti-counterfeiting.

Spontaneous formed dynamic surface wrinkles with tunable morphology and high response attract increasing attentions in the past decades[1]. Taking the advantage of extreme strain-sensitivity, dynamic surface wrinkle patterns have been widely adopted in mechanical enhancement[2,3], soft optics[4,5], electronics[6,7] and sensors[8,9]. As the most important dynamic wrinkling materials, stimulus-response polymers (SRPs)[10] endow the surface dynamic variation of shape[11,12], wettability[13,14], conductivity[15], and fluorescence[16,17] in response to the input stimuli such as temperature[18], pH[19], humidity[20], chemicals[21] and light[22,23]. However, larger deformation of wrinkle patterns mostly relies on physical interactions and lack of spatial selectivity; chemical reaction induced strain is relatively small, which limits the regulation range or rate of wrinkle patterns. In addition, the output optical signals depend mainly on the light scattering of the wrinkle morphology. Therefore, it is highly desirable to develop a wrinkle system that combines excellent spatial selectivity, adaptable control and diversified optical information.

On the other hand, liquid crystal elastomers (LCEs) feature reversible liquid crystal (LC) phase transition, leading to various observable optical and mechanical transformations across distinct phases[24–26]. Very recently, several breakthroughs have unveiled the immense potential of LCE-based smart patterns on flexible display[27], wearable device[25,28], and information storage[29]. Similarly, the phase-transition-induced large-scale deformation endow LCEs fantastic suitability to fabricate wrinkle patterns with multimode response and dynamic adjustability for above mentioned applications. However, liquid crystal polymers (including LCEs) have only been applied as soft substrates in bilayer wrinkle systems[30–33], treated by plasma and rubbing to form wrinkles without other functions[34], or coated on specific wrinkled substrates to copy as the replicas[35]. Taking the advantages of

[1]School of Materials Science and Engineering, East China University of Science and Technology, Shanghai, China. [2]School of Chemistry & Chemical Engineering, Frontiers Science Center for Transformative Molecules, State Key Laboratory for Metal Matrix Composite Materials, Shanghai Jiao Tong University, Shanghai, China. [3]State Key Laboratory of Separation Membranes and Membrane Processes, School of Textile Science and Engineering, Tiangong University, Tianjin, China. ✉e-mail: skn-08284869@sjtu.edu.cn; ponygle@sjtu.edu.cn; yaoyuan@ecust.edu.cn

large deformation and multi-mode information display, a single layer or gradient layer LCE wrinkle system may realize multi-mode and dynamic tunability with better flexibility and durability in comparison to a traditional laminated wrinkle system, simultaneously overcome the shortages of LCEs, such as coupling of chemical structure, elasto-plasticity, and nonlinear mechanics.

Herein, we present a facile and robust strategy to fabricate dynamic wrinkle patterns on a photo-induced gradient crosslinked LCE surface in large scale (Fig. 1). A photodimerization crosslinked layer is constructed on LCE surface upon UV irradiation, giving rise to higher surface modulus that enables the wrinkle pattern's generation by subsequent stretching-releasing induced LC mesogens' orientation and phase transition. We construct the LCE (namely AnLCE) with synthesized monomer anthracene-containing dithiol ($An(SH)_2$) and some commercially available monomers, including the LC mesogen, chain extender, crosslinking agents and catalyst through one-step thiol-acrylate Michael addition crosslinking (Fig. 1b). The obtained wrinkle pattern with tunable surface morphology, featured fluorescent emission of anthracene moiety, the structural color of the wrinkle pattern and birefringence of oriented LC mesogens, providing three visible modes for the wrinkle pattern. Furthermore, LC mesogen endows anthracene-containing liquid crystal elastomer (AnLCE) thermal and mechanical responsibility to reversibly erase the wrinkle pattern upon heating and recover it by repeating stretching-releasing cycles, and therefore the information of the pattern can be encrypted and decrypted by heating/stretching-releasing cycles (Fig. 1c). This strategy paves a avenue to directly fabricate and manipulate dynamic multi-mode LCE patterns, and provides promising soft materials for large-scale information encryption, anti-counterfeiting, and smart display.

Results

Strategy of phase-transition-induced dynamic wrinkle

The key point of the strategy is to tune the phase transition of LCE by approaches including post crosslinking, temperature, and external strain, as well as manipulate dynamic wrinkles' unidirectional erasure and recovery. Thus, we designed an AnLCE. The anthracene group (An) endows LCE the ability of photo-crosslinking, and the commercial acrylate liquid crystal (RM257) molecule takes the charge of phase-transition-induced large-deformation (Fig. 1a, b). After UV exposure, a gradient photodimerization crosslinked surface layer was constructed on AnLCE film with higher modulus, and therein locks the LC domains in a certain dense network whereas the LC domains in the inner layer keep initial crosslinking density. Upon stretching, all mesogens of the

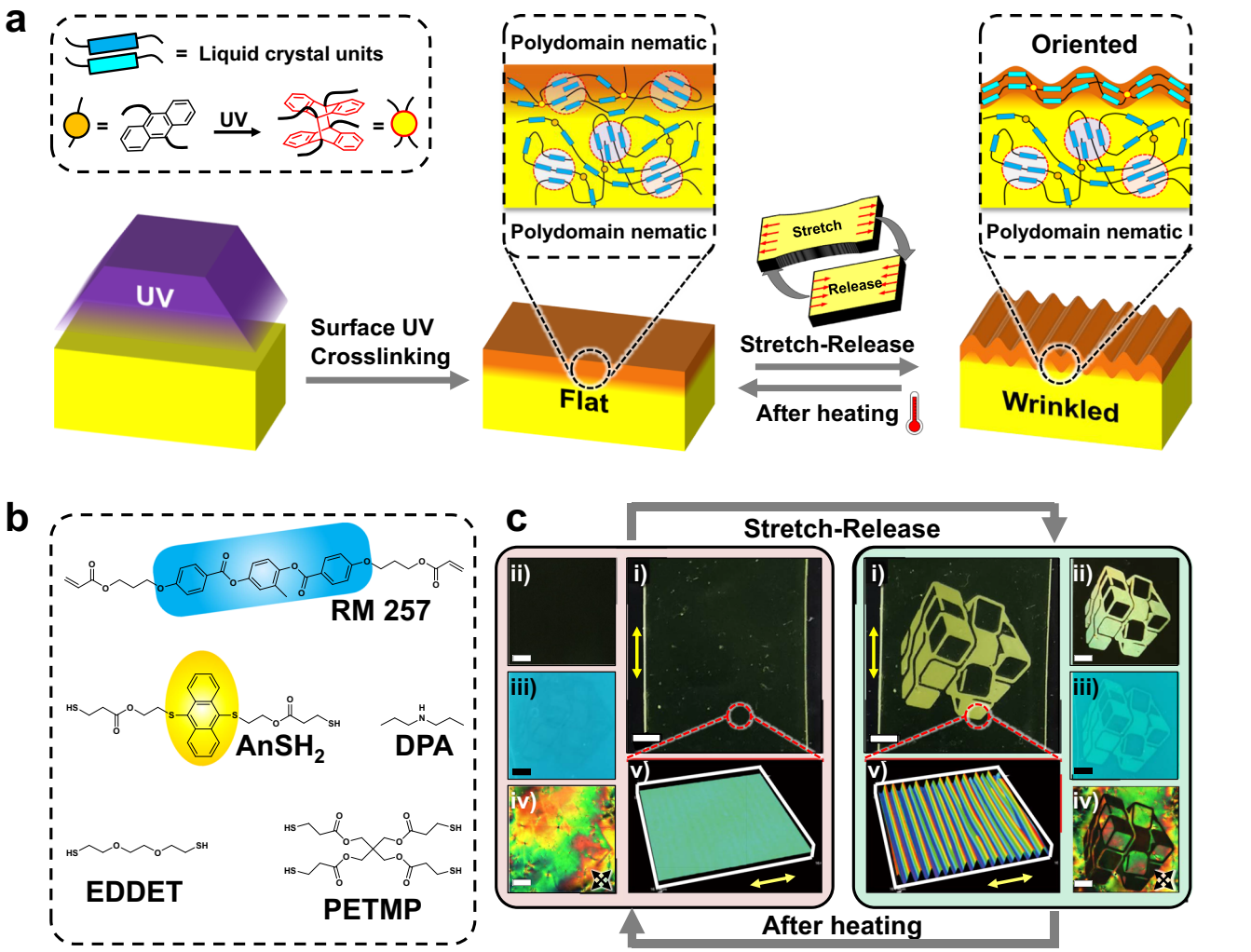

Fig. 1 | Strategy for fabricating surface wrinkle pattern on AnLCE film. **a** Schematic illustration of fabricating wrinkle pattern on AnLCE film and its mechanism for dynamic surface wrinkling. **b** Chemicals for fabricating AnLCE films. **c** Dynamic surface pattern for reversible and multi-mode information display: (i) photograph and (ii) viewing angle dependent structural color under natural light, (iii) fluorescent image under UV and (iv) birefringence patterning under polarized light. While the microstructures in the UV exposed area are shown in (v). The yellow arrows in items (i and v) indicated the direction of the stretching-releasing. Scale bar: 2 mm.

AnLCE are forced to be oriented, but only the mesogens in the inner layer recovers initial polydomain nematic phase while releasing. The LC mesogens in the surface layer still kept orientation due to the high crosslink density. The mismatch of resilience and modulus between the surface layer and inner layer causes buckling on the AnLCE surface. The thin surface layer with high modulus gives rise to unusual fine wrinkles in sub-micro scale, yielding apparent structural color as the recognizable modes of wrinkle patterns together with the fluorescent difference caused by anthracene and polarized sight by oriented LC mesogens (Fig. 1c).

The wrinkle patterns can be unidirectional erased by temperature-controlled phase transition. At a high temperature (above isotropic transition temperature T_{iso}), both the oriented LC mesogens in surface layer and LC polydomain in the inner layer undergo an isotropic transition, resulting in deformation along the oriented direction of top layer and the erasure of wrinkles. The erasure is a unidirectional process since the isotropic LC mesogens in surface layer can only transform into polydomain upon cooling, and the AnLCE's surface will keep flat unless the strip is subjected to stretching-releasing cycles again.

Fabricating wrinkle patterns on AnLCE surface and their evolution

To fabricate phase-transition-induced dynamic wrinkle, we firstly designed and synthesized the photodimerizible monomer $An(SH)_2$ with thiol groups, and then fabricated the photosensitive AnLCE films through thiol-acrylate Michael addition polymerization of diacrylate liquid-crystal monomer (1,4-bis(4-(3-acryloyloxypropoxy)benzoyloxy)-2-methylbenzene, [RM 257]), photo-crosslinkable dithiol (9,10-bis((2-(3-mercaptopropanoyl)oxy)ethyl)thio)anthracene, [$An(SH)_2$]), dithiol chain extender (3,6-dioxa-1,8-octanedithiol, [EDDET]), chain crosslinker (pentaerythritol tetrakis(3-mercaptopropionate), [PETMP]), while the dipropylamine (DPA) and toluene served as catalyst and solvent, respectively, in which RM257 and $An(SH)_2$ were chosen as the liquid crystal unit and photosensitive moiety, respectively (Fig. 1b). The detailed synthesis and characterizations of $An(SH)_2$ were shown in Supplementary Information, and the successful synthesis of $An(SH)_2$ was verified by proton nuclear magnetic resonance spectroscopy (^{1}H NMR) and MS spectra (Supplementary Figs. 1–4). The polymerization process of AnLCE was monitored by Attenuated Total Reflectance Fourier Transform Infrared Spectroscopy. As shown in (Supplementary Fig. 5), the decrease of S-H bending (2570 cm^{-1}) and asymmetric C = C bending (1635 cm^{-1}) and C-H stretching (810 cm^{-1}) peaks revealed consumption of these groups, therefore indicated the polymerization was in process. The resulting crosslinking network in the AnLCE films was then confirmed by swelling tests in dichloromethane (DCM) and the calculated high gelation fraction (~97%) (Supplementary Fig. 6 and Supplementary Table 1). In addition, thermogravimetric analysis (TGA) was employed to verify the thermal stability of the AnLCE film, with the decomposition temperature (T_d) at approximately 300 °C. (Supplementary Fig. 7), which further confirmed the successful fabrication of AnLCE films.

The liquid crystal phase of AnLCE film at room temperature was investigated by polarized optical microscopy (POM) and X-ray diffraction (XRD). The AnLCE film exhibited bright birefringence upon at all angles of rotation with respect to the polarized analyzer, indicating that the film was in polydomain phase with microscopic orientation but macroscopic disorder (Supplementary Fig. 8). A diffusion ring in the wide angle region in the 2D-WAXS pattern and a single diffraction peak found at 20° in the 1D-XRD spectrum further supported the non-oriented polydomain nematic phase. (Supplementary Fig. 9). Dynamic mechanical analysis (DMA) spectrum revealed that the glass transition temperature (T_g) of AnLCE is about 13 °C, while the isotropic transition temperature (T_{iso}) is around 55 °C (Supplementary Fig. 10). The isotropic transition was also corroborated by POM upon heating. As shown in Supplementary Fig. 11, the birefringence of the AnLCE film under polarized light disappeared and transformed into a dark field while heating above T_{iso}. These results demonstrated the LC phase transition of AnLCE film and provided potential for manipulating the surface pattern in subsequent sections.

After the successful fabrication of AnLCE films, the method "UV-SR" was employed to generate wrinkle pattern on the surface of AnLCE. An AnLCE film was exposed to 365 nm UV light at an intensity of 35 mW cm^{-2} for 600 s (this process was named "UV"). During UV exposure, the decrease in the absorption peaks of anthracene at 350–420 nm in the UV-vis spectra indicated that the photodimerization of anthracene was progressing (Supplementary Fig. 12). It resulted in a gradient crosslinking from top layer with higher modulus to inner layer. Atomic force microscopy further demonstrated the depth-dependent cross section modulus variation, indicating the thickness of top layer with high-modulus of 180 MPa was approximately 0.5 μm (Supplementary Fig. 13). After UV exposure, the film was stretched to a 100% elongation and subsequently released to its original length (named "SR"). As shown in Fig. 2a, b, no wrinkle formed on the surface upon stretching, while surface wrinkle appeared during releasing due to the different strain behaviors of the top layer and inner layer. To confirm the difference in stretching-releasing behavior of top layer and inner layer, the mechanical properties of fully UV dimerization-crosslinked film and untreated AnLCE film were studied. As shown in Fig. 2e, following the application of a 100% strain and subsequent release of stress, the crosslinked film demonstrated a lack of capacity to recover its original length, with a residual strain of ~30%. In contrast, the unexposed film showed satisfied recovery with a residual strain of less than 10%. As a result, the difference in recovery between the top layer and the inner layer resulted in the mismatch in compressive strain and generated compressive stress along the SR direction, finally causing the wrinkle formation on AnLCE surface. Besides, it is possible to localize the wrinkled area by using a photomask in UV exposure[32,33,36] and to alter the orientation of the wrinkle by varying the SR direction[37] (Supplementary Figs. 14–15). Once the wrinkle formed on AnLCE surface, the exposed area could be seen by naked eyes due to the strong scattering to light, and the structural color depend on viewing angle was also observed because of the periodic surface structure (Supplementary Movie 1). Therefore, the surface wrinkle was successfully fabricated via the UV-induced gradient crosslinking and subsequent mechanical-induced surface instability.

The detailed evolution of surface wrinkle during releasing was monitored by laser scanning confocal microscopy (LSCM, Fig. 2b). Once the film releasing from $2L_0$, the surface periodic folding-like structure emerged, and the folds increased in amount with the decreasing film strain, until the film reverted to its original length (L_0). After repeated stretching-releasing cycles (SR cycles), the surface structure turned into a sinusoid-like wrinkle morphology with uniform wavelength (λ) and amplitude (A) in their profile along the SR direction (Fig. 2b). In comparison to the wrinkles generated in the initial round of stretching-releasing, the wrinkles formed by repeating the SR cycles were of a shorter wavelength and smaller amplitude. The folding-to-wrinkle transformation was supposed as the result of the redistribution in the buckling surface. After obtaining the uniform wrinkle by SR cycles, its storage stability was subsequently tested, which showed that our obtained wrinkle pattern had good stability and its wrinkle morphology remained almost unchanged during storage for 15 days under room conditions (Supplementary Fig. 16).

Furthermore, we conducted a series of experiments to investigate the factors affecting the wrinkled morphology. As shown in Fig. 2c, d, with the stretching ratios varying from 50% to 150%, the wavelength decreased from 1.24 to 0.77 μm. The amplitude reached a maximum value of 0.42 μm at 100% strain and decreased slightly to 0.34 μm with further increase in strain. In other words, the aspect ratio (A/λ) increased as the strain increased to 100%, while at larger stretching ratios, the surface wrinkles evolved into smaller wrinkles with a similar

https://doi.org/10.1038/s41467-024-55180-3

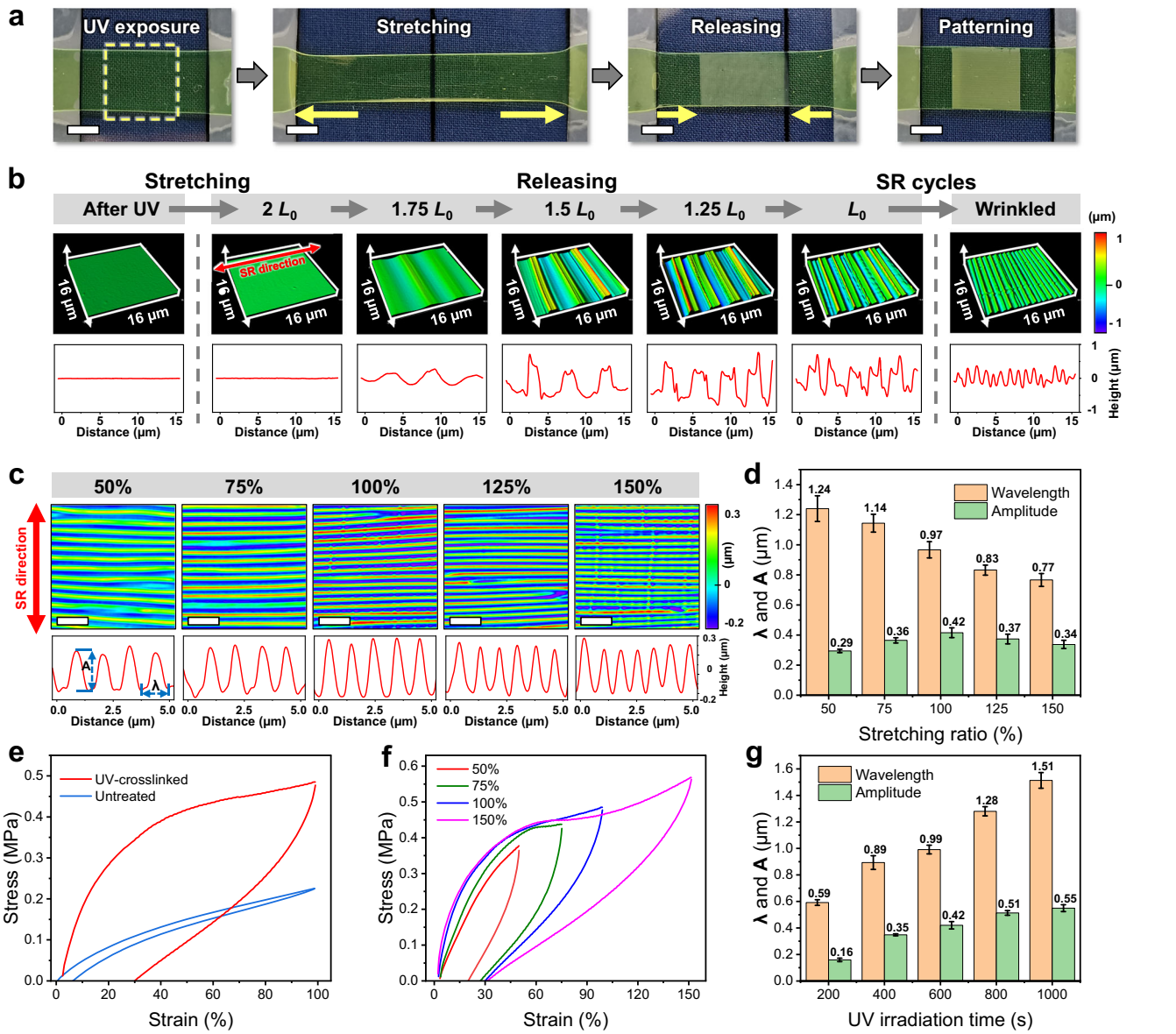

Fig. 2 | Fabrication and evolution of the surface wrinkle patterns. a Photograph of fabricating surface wrinkle on AnLCE film by "UV-SR". Scale bar: 0.5 cm. **b** The evolution of surface structure and their profile along the SR direction under first releasing and after stretching-releasing cycles. In this section, UV exposure time was controlled as 600 s, while the stretching ratio is 100%. "SR cycles" means multi-times stretching-releasing. **c** The evolution of surface wrinkle and their corresponding profile to increasing stretching ratio. In this section, UV exposure time was kept as 600 s, the intensity was 35 mW cm^{-2}. Scale bar: 4 μm. **d** The statistical data of characteristic wavelength and amplitude variation to increasing stretching ratio corresponding to (**c**). Results are shown as mean ± SD, $n = 6$. **e** Strain behaviors of UV-crosslinked (red) and untreated (blue) AnLCE films at 35 °C. **f** Strain behaviors of UV-crosslinked AnLCE films in different stretching ratio at 35 °C. **g** The statistical data of characteristic wavelength and amplitude variation with increasing UV exposure time. In this section, stretching ratio is 100%, the UV intensity was 35 mW cm^{-2}. Results are shown as mean ± SD, $n = 6$.

aspect ratio. The elastic recovery associated with the plastic deformation of crosslinked top layer during releasing was considered as the reason of this phenomenon. As described in Supplementary Discussion, the residual strain of crosslinked layer along the stretching direction was calculated by arc integral (Supplementary Note 1 and Supplementary Eq. 4). According to the calculations, the residual strain of top layer along SR direction increased by increasing the stretching ratio, and kept unchanged when stretching ratio was higher than 100% (Supplementary Table 2). These results corresponded to the strain behavior of UV-crosslinked AnLCE film in stretching-releasing cycle. The residual strain of the crosslinked film increased as the applied elongation increased, and achieved an almost fixed value (about 30%) when the applied elongation was higher than 75% (Fig. 2f). The residual strain may be owing to the limited mobility of liquid crystal domains caused by high-density crosslinking points, making it difficult to keep up with the rapid changes in polymer chain segments during the stretching recovery cycle.

The evolution of wrinkles with UV irradiation time was shown in Fig. 2g and Supplementary Fig. 17. The surface wrinkles' wavelength and amplitude grew from 0.59 to 1.51 μm and from 0.16 to 0.55 μm, respectively, with the increase of the exposure duration (200–1000 s). Longer exposure time led to the denser crosslinking, and therefore increased the thickness and modulus of top layer, resulting in the increasing wavelength and amplitude of wrinkle simultaneously (Supplementary Eqs. 5 and 6)[38]. Therefore, the stable micro-sized surface wrinkle was successfully fabricated on the AnLCE surface, and

https://doi.org/10.1038/s41467-024-55180-3

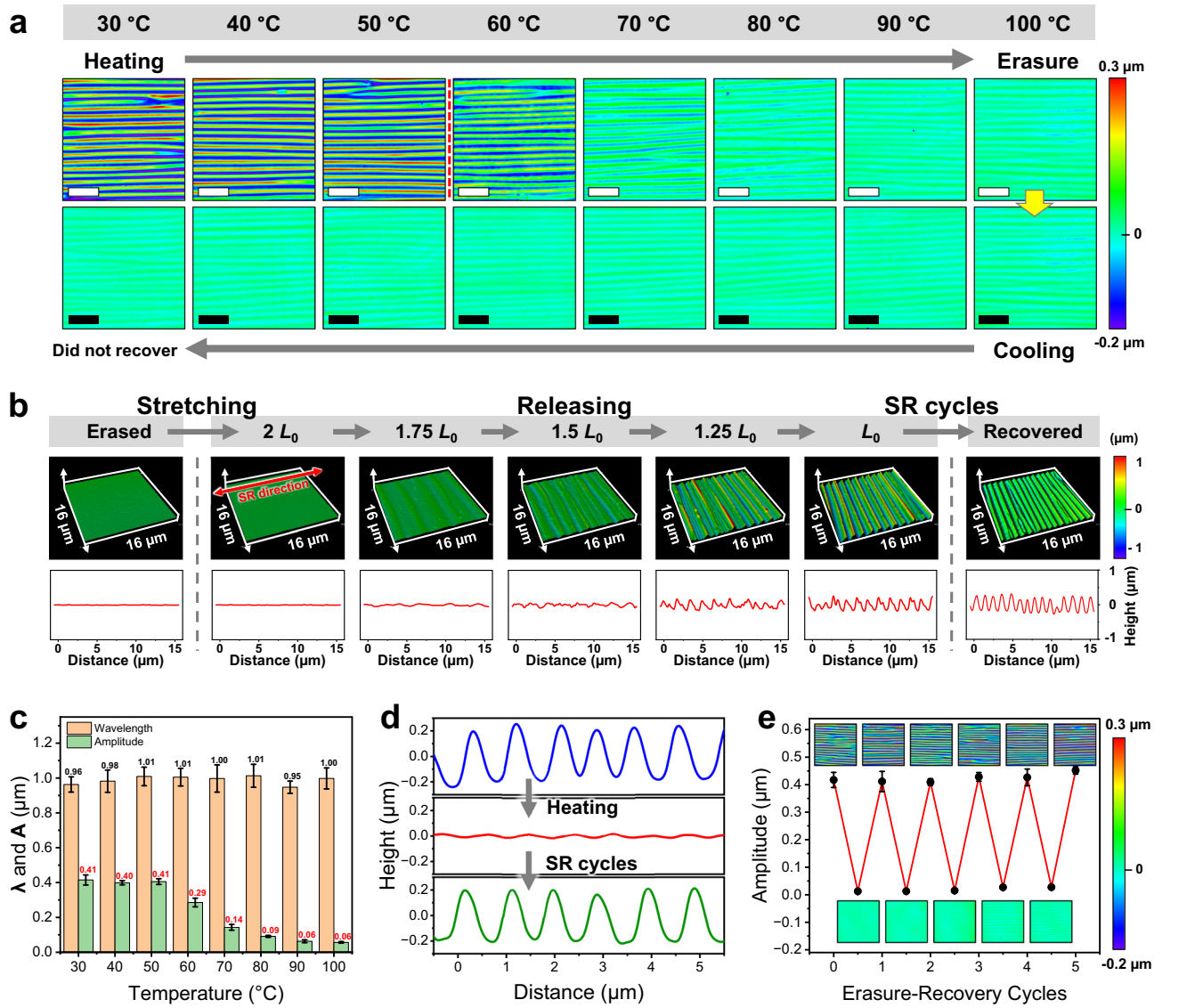

Fig. 3 | Dynamic manipulation of surface wrinkle patterns. a The evolution of AnLCE surface wrinkle morphology upon heating-cooling cycle. Scale bar: 4 μm. **b** The recovery of surface wrinkle under releasing and after stretching-releasing cycle. **c** The evolution of surface wrinkle's characteristic dimensions (wavelength and amplitude) upon heating. **d** Cross-section profiles of surface wrinkles before erasure (blue line), after thermal erasure (red line), and after recovery (green line). **e** Variation of amplitude values under erasure-recovery cycles. The insets are the 2D pattern of the surface morphology. Results are shown as mean ± SD, $n = 6$.

the characteristic dimension could be controlled by both stretching ratio and UV exposure time. In addition, due to the high aspect ratio and short wavelength, these obtained 1D periodic wrinkle patterns can generate structural colors, which could be used as a viewing enhancement of surface information by varying the viewing angle (Fig. 1c).

Dynamic manipulation of surface wrinkle pattern

Dynamic surfaces with tunable microstructure in response to external stimuli show potential in a wide range of applications[39–41]. While LCEs with the phase-transition-induced large-scale deformation provided a feasibility to regulate the surface microstructure. In this work, the generated wrinkle on the surface of AnLCE exhibited favorable response to thermal and mechanical stimuli that could be erased by heating and recovered after SR cycle (Supplementary Movie 2). The erasure and recovery process were monitored by LSCM (Fig. 3a, b). Upon heating, an obvious fading and disappearance were observed at 60 °C and 80 °C, respectively (Fig. 3a). The amplitude was found to decrease from 0.40 to 0.05 μm approximately in the process of erasure by heating, while the wavelength kept constant at around 1 μm (Fig. 3c). During cooling, the wrinkles did not recover, with the same wavelength and amplitude as the erased state at 100 °C (Supplementary Fig. 18). This phenomenon of the unidirectional erasure of wrinkle is owing to the thermal phase-transition-induced deformation of crosslinked top layer. To verify it, we fabricated an individual full-crosslinked AnLCE film to investigate the thermal deformation (Supplementary Fig. 19). After heated to 100 °C, a fully crosslinked AnLCE film, with ~30% residual strain fabricated by stretching to 100% and releasing, contracted to initial length L_0, and remained after cooling to room temperature. This result visualized the occurrence of thermal deformation in the crosslinked top layer, which decreased the necessary compress stress to form wrinkles between top layer and inner layer. Therefore, the erasure of surface wrinkle was demonstrated to be caused by the thermal deformation of the crosslinked top layer. Coincidentally, the onset temperature of erasure was consistent with T_{iso}. Therefore, the liquid crystal phase transition upon heating was supposed as the cause

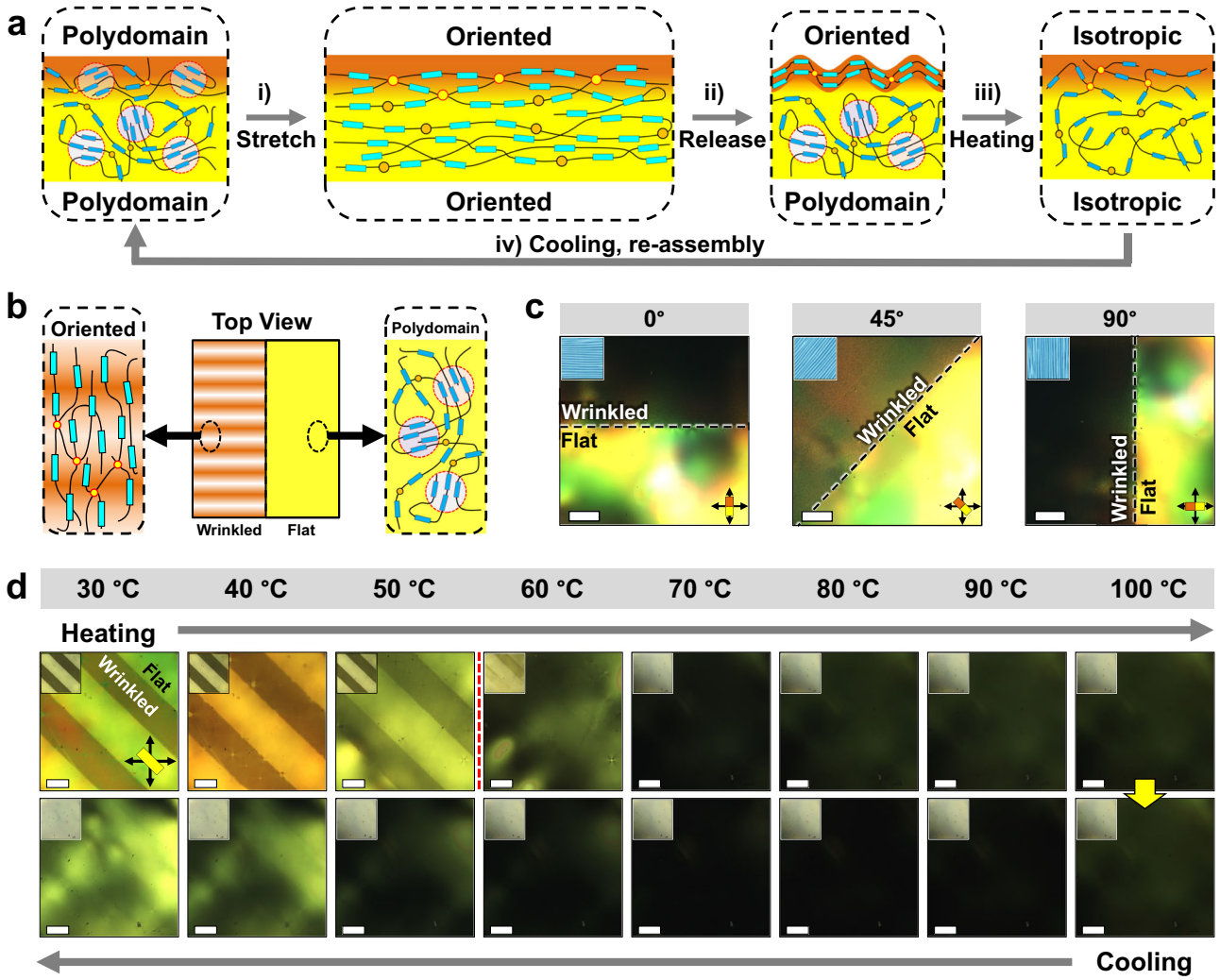

Fig. 4 | Mechanism of dynamic wrinkle patterns induced by liquid crystal transition. a The proposed scheme for liquid crystal alignment evolution in AnLCE film before stretching, under uniaxial stretching, after releasing and under heating above isotropic transition temperature. **b** Hypothesized top view and corresponding molecular alignment of the in wrinkled (exposed area) and flat surface (unexposed area). **c** POM view of the wrinkled and flat area. Scale bar: 200 μm. **d** POM view of the AnLCE film with alternately wrinkled and flat area upon heating-cooling cycle. Insets are the corresponding optical microscopic view. Scale bar: 200 μm.

inducing contraction of top layer and erasure of wrinkles. Detailed demonstration of this supposition will be discussed in the next section. After the wrinkle pattern was erased, the loss of surface contrast between exposed and unexposed areas lead to the visibility of patterned images by naked eyes or optical microscope (Fig. 1c and Supplementary Fig. 20). Typically, if the wrinkled film was directly placed at 100 °C, the wrinkle pattern would be erased within 10 s (Supplementary Movie 2). The rapid response provided an immediate processing to the surface pattern.

The erased wrinkle could only be recovered by SR cycles. As shown in Fig. 3b and Supplementary Movie 2, when the erased surface was re-stretched to $2L_0$ and released, the wrinkle structure appeared again. Similar to the initial flat film (Fig. 2b), folding-like structures formed on the erased film in the first releasing and evolved into sinusoid-like wrinkles after repeating SR cycles (Fig. 3b). However, the regenerated folding-like structures in the first SR cycle was much smaller and more uniform than that on the initial film, and the final uniform wave-like wrinkles after repeating SR cycles were as same as that on the original film. We speculated that the residual wrinkle structure after erasure, even at a very small aspect ratio (Fig. 3d), provided a guidance for the recovery of the sinusoidal wrinkle surface.

The heating-induced erasure and SR recovery of wrinkles exhibited high cycling stability. We further performed erasure-recovery cycles for at least 5 times (Fig. 3e). When the wrinkled AnLCE film was heated to 100 °C, the wrinkle was erased with amplitude decreased. After SR cycles, the wrinkle reappeared with the amplitude recovered to its original value of 0.4 μm without any attenuation. The erasure-recovery cycles verified the cyclic stability of the wrinkles. The acceptable stability, rapid response and well-reversibility of the wrinkle pattern demonstrated that the surface pattern might be available for information encryption and display.

Mechanism for dynamic surface wrinkle pattern via liquid crystal transition

We proposed a mechanism of phase-transition-induced dynamic wrinkle and conducted a series of experiments to get insight into the phenomenon of unidirectional erasure and recovery of surface wrinkle. As shown in Fig. 4a, the aggregation and phase transition of liquid crystal in AnLCE films were proposed as key factors in the stable formation and dynamic transition of surface wrinkle. Initially, the as-prepared AnLCE film was confirmed in a polydomain nematic phase. (i) Upon tensile stress, the mesogens in the whole film were forced to be

oriented along the stretching direction. (ii) Due to the difference in strain response between the crosslinked surface layer and the soft inner layer, the surface buckled during releasing and wrinkles formed, in which the LC mesogens reserved their orientation parallel to the wrinkle wave. Meanwhile, mesogens in the inner layer returned to polydomain state (the top view was illustrated in Fig. 4b). (iii) Heating exceeded T_{iso} gave rise to the LC phase isotropic transition in AnLCE, and therefore resulted in the erasure of wrinkles. (iv) Upon cooling to room temperature, the LC mesogen re-assembles to the polydomain nematic phase, but not the monodomain. This is because the transition from polydomain to monodomain is an entropy-decrease process, which means that the wrinkle will not automatically generate unless it is SR treated again.

To verify the functions of liquid crystal, we designed an amorphous controlled elastomer (AnE) without LC mesogens (the acrylate monomer RM 257 was replaced by PEGDA, Supplementary Fig. 21), where the amorphous phase of the AnE was confirmed by POM (Supplementary Fig. 22). As a result, wrinkle pattern cannot be generated on the AnE film by UV-SR, confirming the necessary of LC mesogens in the formation of wrinkles (Supplementary Fig. 23). Furthermore, to illustrate the effect of LC mesogens in the thermal erasure of wrinkles, one more controlled experiment was conducted, in which wrinkles are fabricated by stretching-UV exposure-releasing (S-UV-R) process on both AnLCE and AnE films. Results show that wrinkles on AnE film could not be erased by heating (Supplementary Fig. 24), while wrinkles on AnLCE exhibited the unidirectional thermal erasure characteristic (Supplementary Fig. 25). These results indicated that the liquid crystal is the key factor in providing the wrinkle surface stability from UV-SR and endowing the thermal response.

To further illustrate the orientation of mesogens during the whole dynamic process of wrinkles, we designed a film with region-selected wrinkles by utilizing photomasked UV exposure. After SR cycles, wrinkle formed on the exposure area, while the unexposed area kept flat. As shown in Fig. 4c and Supplementary Movie 3, the wrinkled area was in lowest brightness under POM when parallel and perpendicular to the analyzer, and showed a bright birefringence at the angle of 45° with respect to the analyzer, which revealed that LC mesogens in wrinkled area were oriented. While the flat area kept in bright birefringence at all angle, indicating that the flat area was in a polydomain phase with macroscopically isotropic. The further small angle X-ray scattering (SAXS) experiment confirmed the orientation of the UV-crosslinked layer after stretching-releasing, while the non-irradiated layer returned to initially non-oriented polydomain phase, which are shown in Supplementary Fig. 26.

The color-variable surface under polarized light by rotating viewing angle is expected to be applied as one of the viewing modes for multi-mode information display. In contrast, the wrinkled AnE surface, fabricated by S-UV-R, exhibited dark pattern in all viewing angle (Supplementary Fig. 24d). The result also proved the AnLCE wrinkle surface's brightness variation under POM is caused by the orientation of liquid crystal rather than the parallel-aligned wrinkle structure. Furthermore, an alternating wrinkle pattern on AnLCE film was monitored under POM during the heating erasure and cooling to illustrate the LC phase transition (Fig. 4d and Supplementary Fig. 27). The polarized sight turned to dark field and the wrinkle pattern was erased when the film was heated exceeding T_{iso}, showing the LC mesogens underwent isotropic phase-transition. In cooling process, the recovery of birefringence induced by the transition to polydomain was observed below 50 °C whereas the stripe-shaped polarized images never reappeared, which was in good accordance with the LC phase transition mechanism. Based on these results, the mechanism of phase-transition-induced dynamic wrinkle was successfully demonstrated as the stabilization from liquid crystal's aggregation and its transition between polydomain and oriented phases.

Dynamic surface wrinkle pattern for dynamic and multi-mode display

As the development of anti-counterfeiting materials, SRPs, with the dynamic abilities, such as color variation[42–45], light emission[44–46], deformation[47,48], incorporated with the switchable information in response to external stimuli are promised as low-cost, high-level safety multi-mode or multi-level anti-counterfeiting methods. Taking the advantage of dynamic character and multiple display modes of above-mentioned wrinkles, we demonstrate a facile and robust method to fabricate dynamic and multi-mode anti-counterfeiting wrinkle pattern on AnLCE. As shown in Fig. 5a, i) The information was encoded by masked UV exposure. In this step, the information was invisible because the wrinkle has not been generated. (ii) After SR cycles, the information was decrypted and available to be observed in different display modes. (iii) The information turned into encrypted state again by the heating erasure of wrinkle. The encryption-decryption cycle enabled the dynamic multi-mode information repeatedly shown on AnLCE's surface.

By utilizing the high spatiotemporal resolution of light, photomasks with various patterns were applied to fabricate hierarchical surface patterns on AnLCE with macro-sized images correlative to photomasks and oriented micro-sized wrinkle (Fig. 5b). The obtained patterns showed multiple visions in different viewing scenarios. In natural sight, the strong contrast between the wrinkled part with flat part could be seen by naked eyes due to the light scattering of wrinkle (under the optical microscope, the wrinkle area was dark, because of the scattering to the vertically incident light). The structural colors induced by micro-sized periodic wrinkle were also an obvious character of wrinkled part. Furthermore, the wrinkle area scattered bright cyan light, while the flat area emitted blue fluorescence upon UV irradiation. When the film was observed under polarized light, the pattern varied its birefringent pattern with rotating the angle. The flat area (in polydomain state) kept constantly bright, whereas the wrinkled area (in orientated state) showed an alternating dark-bright birefringent pattern (Supplementary Movie 4). The polarized sight could also be observed by placing patterned films between two crossed polarizers (Supplementary Fig. 28). Through this simple but feasible method, various complex patterns like alphabet, Rubik's cube had been successfully fabricated and observed, further demonstrating the versatility and generality of this strategy (Fig. 5b and Supplementary Fig. 28).

The dynamic nature of wrinkled pattern enabled the facility in fabricating large-scale pattern with multi-mode surface dynamic information in "encoding-decryption-encryption" cycle. As shown in Fig. 5c. An encoded AnLCE film displayed a "star and leaf" pattern by initial photomasked UV exposure and subsequent SR cycles. The same information was available to be identified under natural light, UV irradiation, or in polarized sight. The pattern was rapidly erased within 10 s at 100 °C, and the information was hidden to guarantee a safety transfer. When the wrinkle was recovered by SR cycles, the information was re-decrypted with multiple display modes (Fig. 5c and Supplementary Movie 5). Because the encryption and decryption were in separated manners (heating and SR cycles), the on-off states were on-demand switched to further guarantee the information security. In contrast to other reported methods, our strategy featured two advantages: (1) The encoding process was simple and low cost with only photomask and UV light. (2) The decryption and encryption were on-demand controlled and easy to operate with acceptable stability.

Discussion

In conclusion, we demonstrated a feasible and robust strategy for dynamic wrinkling on an anthracene-containing LCE film by photo-induced gradient crosslinking and subsequently mechanical-induced surface instability, which possess on-off switchable multi-mode

https://doi.org/10.1038/s41467-024-55180-3

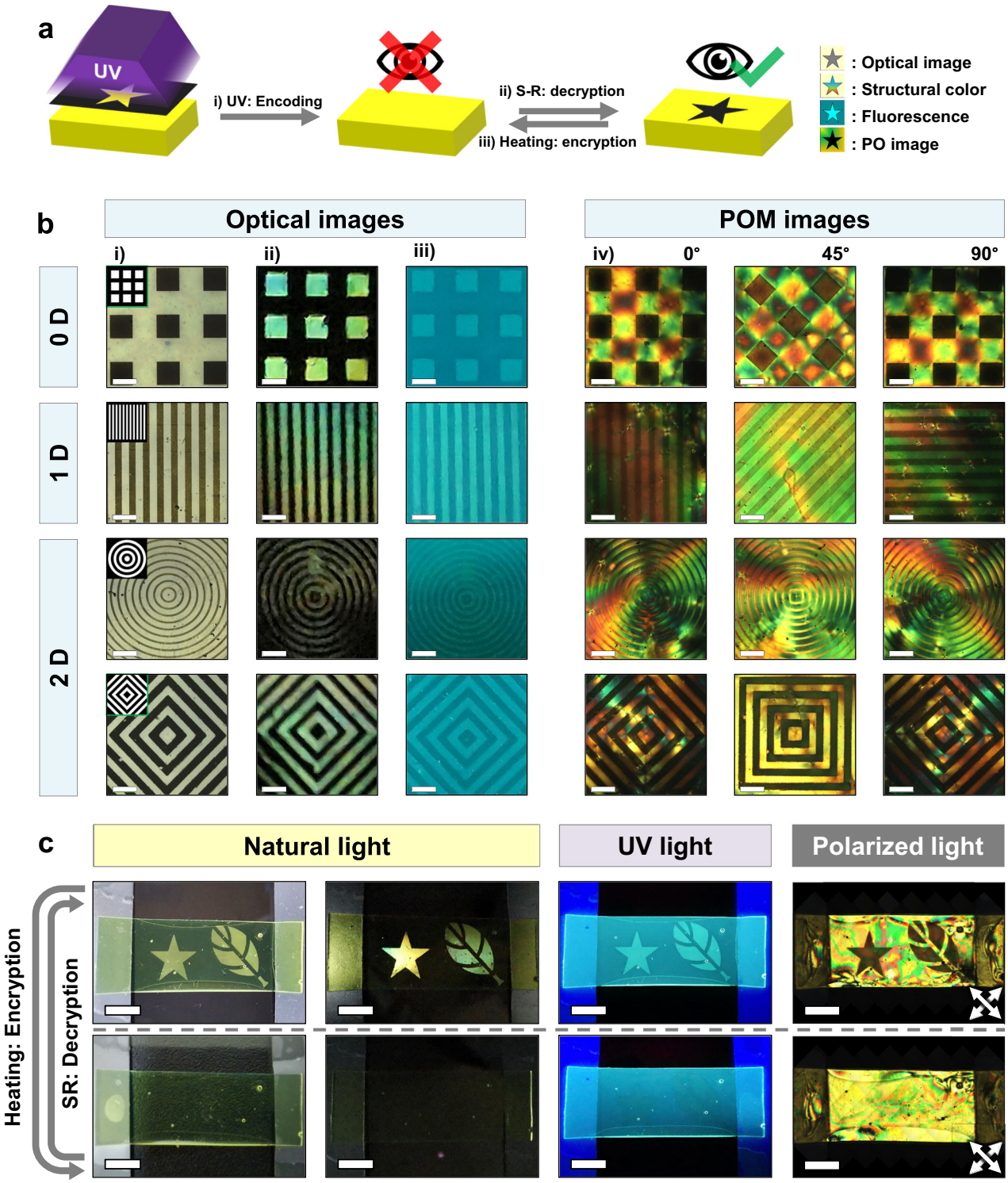

Fig. 5 | Dynamic surface pattern with multi-mode display for information decryption and encryption. a Schematic illustration of information encoding, decryption and encryption on AnLCE film. **b** Various patterns in multi-mode display on AnLCE surface. (i) optical view in natural light, (ii) viewing angle dependent structure color, i(ii) fluorescence under UV light and (iv) PO images under polarized light in different viewing angle. Scale bar: 500 μm. **c** Dynamic and multi-mode pattern for displaying and hiding information. Scale bar: 0.5 cm.

information via phase-transition-induced dynamic surface microstructure. The wrinkle size could be tuned a by exposure time and stretching ratio. The liquid crystal phase transition played a vital role in stabilizing and dynamic regulation to the surface wrinkle by transformation among polydomain nematic, oriented and isotropic phases under the mechanical and thermal manipulation. The dynamic and multi-mode surface encoded with various information showed amazing on-demand switched on/off state to encrypt and decrypt the surface information by heating and SR cycles. This strategy provided a path to modify LCEs' surface and regulating polarized light by

wrinkling, and the facility of this strategy is promising in soft sensors, smart windows and anti-counterfeiting.

Methods

Preparation of AnLCE Film

The synthesis of functional monomer, $An(SH)_2$, was described in Supplementary Information. Nematic LCEs with UV-sensitive anthracene crosslinker (AnLCE) was synthesized by one-step Thiol-Acrylate Michael Addition Polymerization (TAMAP). In this work, the mole ratio of thiol groups and acrylate groups were kept to 100/100. 2 mmol of RM257, 0.8 mmol of $An(SH)_2$ were placed in an 8 mL glass vial, after 0.8 g of toluene was added in, the bottle was heated to 80 °C and stirred till the contents in the vail transferred from solid to clear liquid. And then, thiol monomers, 0.8 mmol of EDDET and 0.2 mmol of PETMP was added in and fully stirred for 5 min. After that, 200 mg of DPA/toluene solution (DPA was diluted as 2 wt% in toluene) was added as a catalyst for TAMAP. The solution was strongly stirred for 1 min and poured into a glass mold, which is with the size of 60 mm × 60 mm × 0.5 mm. The mixture turned into gel with the reaction ran for 24 h at room temperature. After the reaction was completed, the film was heated to 80 °C at a vacuum oven for 24 h for removing the solvent and DPA.

Fabricating wrinkle pattern on the surface of AnLCE Film

The AnLCE films were irradiated with a 365 nm LED light at an intensity of 35 mW cm^{-2} for 600 s unless otherwise stated. Photomask in different patterns were applied. After UV irradiation, the strips were repeatedly stretched to 100% strain and released to its original length for several cycles, patterns on the AnLCE films surface corresponding to the photomask appeared with the surface wrinkle generated. The uniformed wrinkle surfaces were all obtained by repeating the SR cycles.

Strain behavior of UV-crosslinked AnLCE film and untreated AnLCE film

The UV-crosslinked AnLCE film was obtained by fully irradiating a thin AnLCE film (~130 μm) with UV light on both sides for 1 h. By controlling the ambient temperature at 35 °C, the UV-crosslinked AnLCE film and the untreated AnLCE film were stretched to 100% strain at a strain rate of 20%/min followed by a stress release to retract them. Furthermore, the UV-crosslinked AnLCE film was subjected to tensile strain tests at different maximum tensile strains (50% to 150%), with the same ambient temperature and strain rate.

Erasure and recovery of surface wrinkle pattern

To temporarily erased the surface wrinkle, a wrinkled AnLCE films were heated from 30 °C to 100 °C on a heat plate and cooled down to 30 °C. During this session, wrinkle dimension was recorded after 2 min arriving the certain temperature in each 10 °C variation. The wrinkle patterns were recovered by stretching-releasing cycles, with a same stretching strain ratio to that in fabricating wrinkle pattern. Typically, if the wrinkled film was directly placed on a 100 °C heat plate, the wrinkle would rapidly disappear within 10 s.

Characterizations

The strain behaviors of UV-crosslinked AnLCE film and untreated AnLCE film were tested using a dynamic mechanical analyzer instrument (Discovery DMA 850, TA Instruments, America). The surface morphologies in microscale were observed via Laser Scanning Confocal Microscope (LSCM) (Olympus OLS5000 SAF, Olympus, Japan). The polarized optical images were also acquired via the LSCM by switching to the reflection POM mode. The structural color and fluorescent patterns of AnLCE film were acquired by a digital camera under natural light and UV lamp, respectively. SAXS experiments were conducted on an Xeuss 2.0 WAXS/SAXS system (Xenocs, France). The wavelength of X-ray was 0.154 nm. And the X-ray detector was Pilatus 3 R 300 K, with single pixel size was 172 μm. During experiment, the distance between sample and detector was set to be 538.1 mm, and samples underwent X-ray exposure for 300 s. The scattering data of AnLCE films were acquired (1) before stretching, (2) under 200% stretching ($3L_0$) and (3) after releasing to their original length, respectively.

Data availability

The authors declare that the data supporting the findings of this study are available within the paper and its supplementary information files. Source Data are available with the manuscript. Data is also available from the authors on request. Source data are provided with this paper.

References

1. Liu, N. et al. Wrinkled interfaces: taking advantage of anisotropic wrinkling to periodically pattern polymer surfaces. *Adv. Sci.* **10**, 2207210 (2023).
2. Lin, G. et al. Self-similar hierarchical wrinkles as a potential multifunctional smart window with simultaneously tunable transparency, structural color, and droplet transport. *ACS Appl. Mater. Interfaces* **9**, 26510–26517 (2017).
3. Li, J. et al. Self-wrinkling coating for impact resistance and mechanical enhancement. *Sci. Bull.* **68**, 2200–2209 (2023).
4. Jiang, B., Liu, L., Gao, Z. & Wang, W. A general and robust strategy for fabricating mechanoresponsive surface wrinkles with dynamic switchable transmittance. *Adv. Opt. Mater.* **6**, 1800195 (2018).
5. Chen, S. et al. Dynamic metal patterns of wrinkles based on photosensitive layers. *Sci. Bull.* **67**, 2186–2195 (2022).
6. Yin, D. et al. Two-dimensional stretchable organic light-emitting devices with high efficiency. *ACS Appl. Mater. Interfaces* **8**, 31166–31171 (2016).
7. Yin, D. et al. Mechanically Robust stretchable organic optoelectronic devices built using a simple and universal stencil-pattern transferring technology. *Light Sci. Appl.* **7**, 35 (2018).
8. Ma, T. et al. Dynamic surface wrinkles for in situ light-driven dynamic gratings. *ACS Appl. Mater. Interfaces* **14**, 16949–16957 (2022).
9. Ma, T., Chen, S., Li, J., Yin, J. & Jiang, X. Strain-ultrasensitive surface wrinkles for visual optical sensors. *Mater. Horiz.* **9**, 2233–2242 (2022).
10. Hou, H., Yin, J. & Jiang, X. Smart patterned surface with dynamic wrinkles. *Acc. Chem. Res.* **52**, 1025–1035 (2019).
11. Li, W., Liu, Y. & Leng, J. Harnessing wrinkling patterns using shape memory polymer microparticles. *ACS Appl. Mater. Interfaces* **13**, 23074–23080 (2021).
12. Li, T. et al. Photo-induced spatial gradient network for shape memory polymer with pattern-memorizing surface. *Mater. Horiz.* **9**, 3078–3086 (2022).
13. Wang, Q. et al. Controlled preparation of highly stretchable, crack-free wrinkled surfaces with tunable wetting and optical properties. *Langmuir* **40**, 2102–2110 (2024).
14. Xu, L. et al. Earthworm-inspired ultradurable superhydrophobic fabrics from adaptive wrinkled skin. *ACS Appl. Mater. Interfaces* **13**, 6758–6766 (2021).
15. Qian, J. et al. Multiple regulation of dynamic wrinkles based on conjugated copolymer network. *Sci. China Mater.* **67**, 363–371 (2024).
16. Zhang, L., Bai, J., Ma, T., Yin, J. & Jiang, X. Intelligent surface with multi-dimensional information enabled by a dual responsive pattern with fluorescence and wrinkle. *Macromolecules* **55**, 6405–6414 (2022).
17. Shou, H. et al. Photo-oxidation-controlled surface pattern with responsive wrinkled topography and fluorescence. *Chem. Eur. J.* **27**, 5810–5816 (2021).

18. Hou, H., Yin, J. & Jiang, X. Reversible Diels-Alder reaction to control wrinkle patterns: from dynamic chemistry to dynamic patterns. *Adv. Mater.* **28**, 9126–9132 (2016).
19. Li, J. et al. Light-induced programmable 2D ordered patterns based on a hyperbranched Poly(ether amine) (hPEA)-functionalized graphene film. *ACS Appl. Mater. Interfaces* **13**, 1704–1713 (2021).
20. Zhu, S. et al. Humidity-driven dynamic based on polystyrene-contained Gelatin (Gel-PS) and PDMS bilayer wrinkling system. *Adv. Funct. Mater.* **33**, 2301850 (2023).
21. Zhou, L. et al. Dynamic Interpenetrating Polymer Network (IPN) strategy for multiresponsive hierarchical pattern of reversible wrinkle. *ACS Appl. Mater. Interfaces* **11**, 15977–15985 (2019).
22. Wang, J. et al. Light-assisted anti-wrinkling on Azobenzene-containing polyblend films. *Soft Matter* **18**, 4475–4482 (2022).
23. Li, T. et al. Hierarchical 3D patterns with dynamic wrinkles produced by a photocontrolled Diels-Alder reaction on the surface. *Adv. Mater.* **32**, 1906712 (2020).
24. Yakacki, C. M. et al. Tailorable and programmable liquid-crystalline elastomers using a two-stage Thiol–Acrylate reaction. *RSC Adv.* **5**, 18997–19001 (2015).
25. Choi, S. H. et al. Phase patterning of liquid crystal elastomers by laser-induced dynamic crosslinking. *Nat. Mater.* **23**, 834–843 (2024).
26. Li, Y. et al. Morphing of stiffness-heterogeneous liquid crystal elastomers via mechanical training and locally controlled photopolymerization. *Matter* **5**, 4332–4346 (2022).
27. Wang, H. et al. A dual-responsive liquid crystal elastomer for multilevel encryption and transient information display. *Angew. Chem. Int. Ed.* **62**, 202313728 (2023).
28. Geng, Y., Kizhakidathazhath, R. & Lagerwall, J. P. F. Robust cholesteric liquid crystal elastomer fibres for mechanochromic textiles. *Nat. Mater.* **21**, 1441–1447 (2022).
29. Gao, J., He, Y., Cong, X., Yi, H. & Guo, J. Reconfigurable fluorescent liquid crystal elastomers for integrated visual and haptic information storage. *ACS Appl. Mater. Interfaces* **14**, 53348–53358 (2022).
30. Agrawal, A., Yun, T., Pesek, S. L., Chapman, W. G. & Verduzco, R. Shape-responsive liquid crystal elastomer bilayers. *Soft Matter* **10**, 1411–1415 (2014).
31. Agrawal, A. et al. Surface wrinkling in liquid crystal elastomers. *Soft Matter* **8**, 7138–7142 (2012).
32. de Haan, L. T., Leclère, P., Damman, P., Schenning, A. P. H. J. & Debije, M. G. On-demand wrinkling patterns in thin metal films generated from self-assembling liquid crystals. *Adv. Funct. Mater.* **25**, 1360–1365 (2014).
33. de Haan, L. T. et al. Contactless control of local surface buckling in photoaligned gold/liquid crystal polymer bilayers. *Langmuir* **34**, 10543–10549 (2018).
34. Sim, J. et al. Self-organized wrinkling of liquid crystalline polymer with plasma treatment. *J. Mater. Res.* **33**, 4092–4100 (2018).
35. Lim, S. I. et al. When chirophotonic film meets wrinkles: viewing angle independent corrugated photonic crystal paper. *Adv. Mater.* **35**, 2206764 (2023).
36. Fu, C., Xu, F. & Huo, Y. Photo-controlled patterned wrinkling of liquid crystalline polymer films on compliant substrates. *Int. J. Solids Struct.* **132-133**, 264–277 (2018).
37. Li, Z., Liu, Y., Marin, M. & Yin, Y. Thickness-dependent wrinkling of PDMS films for programmable mechanochromic responses. *Nano Res.* **13**, 1882–1888 (2020).
38. Hou, H. et al. Reversible surface patterning by dynamic crosslink gradients: controlling buckling in 2D. *Adv. Mater.* **30**, 1803463 (2018).
39. Xu, W. C. et al. Designing rewritable dual-mode patterns using a stretchable photoresponsive polymer via orthogonal photopatterning. *Adv. Mater.* **34**, 2202150 (2022).
40. Liu, Y. et al. Fabrication of anticounterfeiting nanocomposites with multiple security features via integration of a photoresponsive polymer and upconverting nanoparticles. *Adv. Funct. Mater.* **31**, https://doi.org/10.1002/adfm.202103908 (2021).
41. Jeon, J. et al. Height-tunable replica molding using viscous polymeric resins. *ACS Macro Lett.* **11**, 428–433 (2022).
42. Zhang, S. et al. Reversible information storage based on rhodamine derivative in mechanochromic cholesteric liquid crystalline elastomer. *Adv. Funct. Mater.* **33**, 2305364 (2023).
43. Liao, J. et al. Multiresponsive elastic colloidal crystals for reversible structural color patterns. *Adv. Funct. Mater.* **29**, 1902954 (2019).
44. Li, L. et al. Finely manipulating room temperature phosphorescence by dynamic lanthanide coordination toward multi-level information security. *Nat. Commun.* **15**, 3846 (2024).
45. Xu, M., Qiu, X., Liang, S., Huang, W. & Zhang, L. Phase-Transition-triggered optical switching for multistage information encryption/decryption. *Adv. Opt. Mater.* **11**, 2201737 (2022).
46. Li, C. et al. Photoswitchable and reversible fluorescent eutectogels for conformal information encryption. *Angew. Chem. Int. Ed.* **62**, 202313971 (2023).
47. Wu, B. et al. Cephalopod-Inspired chemical-gated hydrogel actuation systems for information 3D-encoding display. *Adv. Mater.* **36**, 2401659 (2024).
48. Xie, J. et al. Environment-interactive programmable deformation of electronically innervated synergistic fluorescence-color/shape changeable hydrogel actuators. *Small* **19**, 2304204 (2023).

Acknowledgements

Y.Y. acknowledges the financial support of the National Natural Science Foundation of China (52073094, 52273291), X.J. acknowledges the support of the National Natural Science Foundation of China (52025032) and Shanghai Scientific and Technological Innovation Projects (20ZR1415600), T.M. acknowledges the financial support postdoctoral Fellowship Program of CPSF (GZC20231544). We would like to extend our sincere thanks to Professor Jianqi Zhang of the National Center for Nanoscience and Technology for his help in WAXS characterization.

Author contributions

Y.Y., X.J., T.M., and T. W. conceived the concept and designed the experiments. T.W. and J.Q. characterized the materials, performed the measurements, and wrote the manuscript. Z.S. performed the SAXS experiments and its analysis. Y.Y., X.J., and T.M. supervised the research. All authors contributed to this work.

Competing interests

The authors declare no competing interests.

Additional information

Supplementary information The online version contains supplementary material available at https://doi.org/10.1038/s41467-024-55180-3.

Correspondence and requests for materials should be addressed to Tianjiao Ma, Xuesong Jiang or Yuan Yao.

Peer review information *Nature Communications* thanks Yoshitaka Takezawa and the other, anonymous, reviewers for their contribution to the peer review of this work. A peer review file is available.